Development of an adsorption process for phosphate removal and recovery from municipal wastewater based on hydrotalcite-related materials

C. Maggetti[a], D. Pinelli[a], V. Di Federico[a], L. Sisti[a], T. Tabanelli[b], F. Cavani[b], D. Frascari[a]*

[a] Department of Civil, Chemical, Environmental and Materials Engineering (DICAM), Alma Mater Studiorum – University of Bologna, via Terracini 28, 40131 Bologna, Italy
[b] Dipartimento di Chimica Industriale "Toso Montanari", Alma Mater Studiorum – University of Bologna, Viale Risorgimento 4, 40136, Bologna, Italy
* Corresponding author. Tel: +39 051 2090416. E-mail: dario.frascari@unibo.it.

SUPPLEMENTARY MATERIAL

Text S1. Main features of the tested sorbents.

Commercial HAIX polymeric resin LayneRT

LayneRT is a commercial HAIX (SolmeteX, Massachusetts, USA) manly used for arsenic (As) removal from WW. It consists of a strong base anionic ion-exchange polymeric resin (namely a polystyrene-divinylbenzene macroporous polymer functionalized with quaternary ammonium active sites) that supports a dispersion of ferric oxide nanoparticles, the actual active sites for P adsorption. In this work, HAIX LayneRT was used as a benchmark as its high performance was already assessed in a previous work (Pinelli et al., 2022). It shows an iron content of 75-90 mg as Fe/g_{resin}, a bulk density of 790-840 g/L and its ion-exchange capacity is assessed to be 1 meq/L.

Layered Double Hydroxides (LDH)

Layered double hydroxides (LDH) are a class of ionic solids characterized by a layered structure with the generic layer sequence $[AcB\text{-}Z\text{-}AcB]_n$, where "c" represents layers of metal cations, "A" and "B" are layers of hydroxide anions, and "Z" are layers of other anions and neutral molecules (such as water). Lateral offsets between the layers may result in longer repeating periods. The intercalated anions (Z) are weakly bound, often exchangeable, this last feature makes LDH a interest material for ion adsorption from WW. Two different kinds of LDH materials have been tested for P adsorption in this work: commercial Mg:Al hydrotalcites and Mg:Fe pyroaurite.

Commercial Hydrotalcites – Pural 50 and Pural 70 by Sasol^{RT}

Hydrotalcites, whose name is derived from its resemblance with talc and its high-water content, belong to the class of Layered Double Hydroxides (LDH). The mineral, most stable, hydrotalcite has characterized by the general formula $Mg_6Al_2CO_3(OH)_{16}\cdot 4H_2O$ (Mg/Al ratio equal to three). Multiple structures containing loosely bound carbonate ions exist and the atomic ratio between the bivalent (Me^{2+}) and trivalent (Me^{3+}) cation may vary on a specific range of values depending on the actual ionic radii differences between the two (Cavani et al., 1991). Hydrotalcites Pural is a commercial material by Sasol^{RT} and is available in two variants, named Pural 50 and Pural 70. These two materials primarily differ in their chemical composition and certain physical properties. Pural 50 is composed of 50% magnesium oxide (MgO) and 50% aluminum oxide (Al_2O_3), while Pural 70 has a composition of 70% MgO and 30% Al_2O_3. Both variants contain a carbon percentage ranging from 0.5% to 3%,

and the maximum levels of silica (SiO_2) and iron oxide (Fe_2O_3) are 350 ppm and 200 ppm, respectively. Additionally, impurities of sodium (Na), calcium (Ca), and titanium (Ti) are present in maximum quantities of 50 ppm each. From a physical properties' perspective, Pural 50 has a specific surface area of 2.9 m^2/g, while Pural 70's specific surface area is slightly lower at 13 m^2/g. Both materials have a pore volume of 0.2 ml/g. However, the bulk density varies: Pural 50 has a bulk density ranging from 450 to 650 g/l, whereas for Pural 70 it ranges from 350 to 550 g/l.
Both materials have been tested as shipped (uncalcined Pural 50 and Pural 70) or after thermal treatment at 500°C for 5h (calcined Pural 50 and Pural 70).

Modified Pural 70 with Fe_2O_3

Addition tests were made using an ad-hoc prepared Fe_2O_3 supported over calcined Pural P70, this way trying to increase the adsorption capacity and selectivity towards phosphates. Incipient wetness impregnation (IWI), also known as capillary impregnation or dry impregnation, is a widely used technique for heterogeneous catalyst synthesis. The active metal precursor is typically dissolved in an aqueous or organic solution and then the solution is added dropwise to sorbent (or catalyst support) in a volume corresponding to the estimated pore volume of the solid. The solution is drawn into the pores by capillary action. Then, the impregnated sorbent can be dried up and calcined to remove the volatile components of the solution and deposit the metal on the sorbent surface. The active metal precursor used for the impregnation on Pural 70 hydrotalcite was a metal solution containing 5% wt. of Fe_2O_3. The impregnated sorbent was dried for 1-2 hours at 90°C and then calcined at 2°C/min until 450°C for 5 hours. The calcinated material was pelletized using Specac pelletizer at 1.3 tonn cm^{-2} pressure. The pelletized material obtained was in circular disk space, which was then broken manually and sieved to the desired particle size range (0.355-0.710 mm) for the continuous flow tests in the lab scale and pilot adsorption column.

Pyroaurite

Pyroaurite is a hydrotalcite-like material based on Mg and Fe characterized by the general formula $Mg_6Fe_2(OH)_{16}[CO_3]\cdot 4H_2O$, in which iron replaces aluminum in the hydrotalcite structure.
Pyroaurite has been synthesized by co-precipitation of the metal hydroxides at controlled pH and temperature, a procedure typically used for hydrotalcite synthesis. The co-precipitation procedure was chosen due to its simplicity in procedural methods. The chosen Mg:Fe atomic ratio of three is the stoichiometric one for the hydrotalcites and was chosen to guarantee the formation of a pyroaurite pure phase.
In particular, a solution of magnesium nitrate ($Mg(NO_3)_2\cdot 6H_2O$) and iron nitrate $Fe(NO_3)_3\cdot 9H_2O$ in a molar ratio of 3:1, with cations concentration 1 mol/L in distilled water, was slowly added dropwise at 50°C under vigorous stirring to a solution containing an excess sodium carbonate ($Na_2CO_3\cdot 10H_2O$, 1.2 M concentration in distilled water) compared to the stoichiometric amount required for the formation of the hydrotalcite. The pH of the system was monitored using Amel Instrument 380 and kept at 10.5 by adding 3M NaOH. After the precipitation of the pyroaurite, the solid was aged for 1 hour, then filtered and washed with 2 liters of distilled water at 40°C to remove the nitrates (NO_3^-) from the precipitated solid paste and finally dried overnight at 110°C to obtain the desired pyroaurite sample. Part of the solid was then calcined with a temperature ramp of 5°C/min up to 450°C for 5 hours to promote the thermal degradation of the structure, with a concomitant evolution of both water and CO_2 allowing to obtain a porous mixed-metal oxide structure of Mg and Fe (Mg/Fe/O with a Mg/Fe atomic ratio of 3). Both the dried and calcined materials were pelletized using Specac pelletiser at 1.3 tonn cm^{-2}, crushed and sieved to the desired particle size range (0.355-0.710 mm).

Granular iron hydroxide: FerroSorp® plus

FerroSorp® Plus is a commercial granular iron (III) hydroxide material (a by-product of wastewater treatment) sold by HeGO Biotec, Germany. Because of its chemical activity, iron (III) hydroxide is well suited for the binding of arsenate, phosphate, or sulfide ions in wastewater. Heavy metal ion binding is known to facilitate a combination of adsorption and fixation inside the crystal lattice of ferric hydroxide. Furthermore, there is the possibility of adsorption of organic wastewater constituents that is relatively unspecific. The following simplified equations explain the chemical interactions of phosphate, arsenate, and hydrogen sulfide with ferric hydroxide:

$$ferric\ phosphate:\ \mathrm{Fe(OH)_3 + H_3PO_4 \rightarrow FePO_4 + 3H_2O}$$

$$ferric\ aresnate:\ \mathrm{Fe(OH)_3 + H_3AsO_4 \rightarrow FeAsO_4 + 3H_2O}$$

$$ferric\ sulphide:\ \mathrm{2Fe(OH)_3 + 3H_2\ S \rightarrow 2Fe_2\ S_3 + 6H_2O}$$

Text S2. Isotherm tests: experimental details, model description and best fitting procedure.

The resin concentration was maintained constant at 1 $g_{dry\ resin}\ L^{-1}$, the liquid volume was set to 0.1 L. For each point of the isotherms conducted with WWTP effluent, the desired P initial concentration was reached by mixing 100 mL of effluent with 0.005-1 mL aliquots of different K_2HPO_4/KH_2PO_4 solutions, so as to maintain the effect of dilution of the competing anions at negligible levels (<1%). In each added solution, the K_2HPO_4:KH_2PO_4 ratio was equal to 1:2, in order to maintain the solution pH at 6.8. These solutions were designed so as to attain a total P concentration equal to 9 g L^{-1} (for the solution added to the medium-low concentration points of the isotherms) or 90 g L^{-1} (for the solution added to the high concentration points of the isotherms).
The glass vials were placed in a rotatory shaker (200 rpm, 22°C) for 6 h, to reach the equilibrium condition. The duration of the experiment was defined based on the outcome of the above-described kinetic tests. The P equilibrium concentration in the solid phase, $C_{S,eq}$ was determined as:

$$C_{S,eq} = \frac{\left(C_{L,0} - C_{L,eq}\right) \cdot V_L}{m_S}$$

where: m_S is the mass of the dry sorbent, $C_{L,0}$ and $C_{L,eq}$ the initial and final PO_4-P concentration in the liquid phase and V_L the liquid volume. The tests were performed in triplicates and the 95% confidence intervals associated to $C_{S,eq}$ were calculated from the standard deviation of the mean values.
Experimental isotherms were fitted by means of the Langmuir and Freundlich models.

Langmuir $$C_{S,eq,i} = \frac{C_{S,i}^{\infty} \cdot C_{L,eq,i}}{\frac{1}{K_{eq,i}} + C_{L,eq,i}}$$

Freundlich $$C_{S,eq,i} = K_{F,i} \cdot C_{L,eq,i}^{1/n_i}$$

where: $C_{S,eq,i}$ ($g_i\ g_{dry\ resin}^{-1}$) and $C_{L,eq,i}$ ($g_i\ L^{-1}$) indicate respectively the amount of sorbed *i*-compound per unit mass of adsorbent and the *i*-compound concentration in the liquid phase at equilibrium; $C_{S,i}^{\infty}$ ($g_i\ g_{dry\ resin}^{-1}$) the maximum amount sorbed per unit mass of adsorbent, corresponding to a complete monolayer on the adsorbent surface; $K_{eq,i}$ ($L_{pore\ volume}\ mg_i^{-1}$) the constant related to the affinity between the binding sites and the *i*-compound; $K_{F,i}$ ($mg_i^{1-1/n}\ L^{1/n}\ g_{dry\ resin}^{-1}$) the sorption capacity in the Freundlich model; $1/n_i$ (-) the sorption intensity in the Freundlich model.
The model parameters were estimated by non-linear least squares regression of the calculated the *i*-compound solid phase concentrations ($C_{S,eq,calc,i}$) to the corresponding experimental values ($C_{S,eq,i}$). The best-fitting model was selected based on the correlation coefficient R^2, defined so as to take into account the number of model parameters:

$$R^2 = 1 - \left(\frac{\sum_{i=1}^{N} \left(C_{S,eq,i} - C_{S,eq,calc,i}\right)^2}{N - P - 1} \right) \Bigg/ \left(\frac{\sum_{i=1}^{N} \left(C_{S,eq,i} - C_{S,eq,m}\right)^2}{N - 1} \right)$$

where N indicates the number of experimental tests in the studied isotherm, and P the number of model parameters.

Text S3. Fluid dynamic characterization of the packed columns.

To evaluate the packing quality and the fluid dynamic behavior of the packed bed, a frontal analysis experimental test was carried out after each packing procedure. A 0.5 M NaOH solution was fed from the top of the column at a superficial velocity of 2.4 m h^{-1}. At the column outlet, the electrical conductivity (EC) was measured with a CO11 conductivity probe (VWR, Radnor, Pennsylvania, USA). The packing quality was evaluated by means of two approaches based on the analysis of the retention times distribution curve (RTD) obtained by calculating point by point the derivative of the sigmoidal experimental curve of normalized EC versus time provided by the fluid-dynamic test. The first approach is based on the Theoretical Plate Model: the number of theoretical plates N_{tp} can be evaluated as:

$$N_{tp} = 5.54 \cdot (t_R/w_{1/2})^2$$

where t_R indicates the retention time of the RTD curve and $w_{1/2}$ is width at half-height. The height equivalent to a theoretical plate (HETP) can then be calculated as L/N_{tp}, where L indicates the column length. A high-quality column packing is characterized by a value of $HETP/d_p < 3$, where d_p indicates the average size of the packing particles. The second approach is based on the asymmetry factor (As), defined as the ratio between the leading and tailing semi-width of the peak at 10% of the peak height, and representing the peak deviation from a Gaussian curve. Its value should be as close as possible to 1. The frontal analysis data were also utilized to estimate the effective porosity (e) and longitudinal dispersivity (α_L) of the resin packed bed. The former parameter was evaluated directly from the RTD curve, whereas the latter was estimated by best-fit of the experimental outlet concentrations with a 1-D convection-dispersion model:

$$\delta_i \cdot \frac{\partial C_{L,i}}{\partial t} = -v_{int} \cdot \frac{\partial C_{L,i}}{\partial z} + D_{eq} \cdot \frac{\partial^2 C_{L,i}}{\partial z^2}$$

In the equation above the retardation factor δ_i, equal to $1 + K_{eq,i} \cdot \rho_b/\varepsilon$ was set to 1 due to the absence of NaOH adsorption, the interstitial velocity v_{int} was calculated as $Q/(St \cdot \varepsilon_{resin})$ for the resin bed, and the equivalent diffusion coefficient D_{eq} was approximately expressed as $a_{L,resin}\, v_{int,resin}$.

Text S4. Indicators for the assessment of adsorption performance.

Adsorption performance was assessed by means of the following indicators, calculated at the 1 mg_P L^{-1} breakpoint (BP), unless otherwise indicated in the main article. More information can be found in (Frascari et al., 2016).

$$BV\ of\ MWW\ treated\ = \frac{volume\ of\ WW\ treated\ at\ BP}{adsorption\ Bed\ Volume}$$

$$Adsorption\ yield = \frac{P\ mass\ adsorbed\ at\ BP}{P\ mass\ fed\ at\ BP}$$

$$Sorbent\ utilization\ efficiency = \frac{P\ mass\ adsorbed\ at\ BP}{P\ mass\ sorbed\ at\ bed\ saturation}$$

$$P\ operating\ capacity\ (OC) = \frac{P\ mass\ adsorbed}{mass\ of\ dry\ sorbent}$$

$$Overall\ P\ recovery\ yield\ = \frac{desorbed\ mass\ of\ P}{fed\ mass\ of\ P}$$

Text S5. Simulation of adsorption breakthrough curves with the Thomas model.

The P adsorption breakthrough curves were simulated, both for the lab-scale and pilot plant tests, by means of the Thomas model (Thomas, 1944):

$$C_L(x,t) = \frac{C_{L,0}}{1 + e^{\left[C_{S,eq} \cdot m \cdot \frac{x}{L} - C_{L,0} \cdot Q \cdot t + C_{L,0} \cdot BV \cdot \varepsilon \cdot \frac{x}{L} \cdot \frac{K_{Th}}{Q}\right]}}$$

where $C_L\ (x,t)$ and $C_{L,0}$ ($mg_P\ L^{-1}$) are respectively the P liquid-phase concentrations at height x (m) in the column at time t (h) and the average concentration fed to the column during the test, m (g_{dry}) the mass of dry resin packed in the column, x (m) the zeolite bed height in a generic point of the column, L (m) the maximum zeolite bed height (0.60 m), Q ($L\ h^{-1}$) the flowrate fed to the column, BV (L) the resin bed volume, ε (-) the effective porosity of the packed bed, $C_{S,eq}$ ($mg_P\ g_{dry\ resin}^{-1}$) the resin capacity at saturation (i.e. in equilibrium with $C_{L,0}$) and K_{Th} ($L\ h^{-1}\ mg^{-1}$) the Thomas rate constant. The best-fitting values of $C_{S,eq}$ and K_{Th} were estimated using the Solver add-in in Microsoft Excel, using for the other parameters input values derived from experimental measurements or from elaboration of the fluid-dynamic tests.

Table S1. Main features of the tested sorbents.

Characteristic	**units**	**HAIX LayneRT**	**Pural 50**	**Calcined Pural 50**	**Pural 70**	**Calcined Pural 70**	**Calcined Fe_2O_3-Pural 70**	**Pyroaurite**	**Calcined pyroaurite**	**FerroSorp Plus**
Supplier	--	Layne	Sasol	Sasol	Sasol	Sasol	Sasol + impregnation by University of Bologna	Produced internally at University of Bologna		HeGO Biotec
Structure	--	polymer	LDH	Mg/Al/O	LDH	Mg/Al/O	Mg/Al/O + Fe_2O_3	LDH	Mg/Fe/O	$Fe(OH)_3$
Treatment	--	Impregnation with iron nanoparticles	Dried overnight	Calcination 450°C 5h	Dried overnight	Calcination 450°C 5h	Impregnation of P70 and calcination	Dried overnight	Calcination 450°C 5h	None
Me^{3+}	--	[a]	Al	Al	Al	Al	[a]	Fe	Fe	[a]
Mg/Me^{3+} ratio	--	[a]	1.3	1.3	2.95	[a]	[a]	3	3	[a]
Specific surface area	$m^2 g^{-1}$	[b]	2.9	11	13	8.7	73	44	63	[b]
Bulk density	$g_{dry\ sorbent} L^{-1}$	790-840	450-650	[b]	350–500	[b]	[b]	570-670	[b]	660
Particle diameter	µm	690	[b]	[b]	[b]	355-710	[b]	355-710	355-710	[b]

[a] Not applicable

[b] Not available

Table S2. Comparison of the maximum adsorption capacities of various adsorbent reported in literature.

Adsorbent	P adsorption capacity at infinite conc. in the liquid phase (mg g^{-1})	Range of P liquid phase concentration at equilibrium (mg L^{-1})	Liquid Media Type	References
Calcined Pyroaurite	26.1	0 - 14	Real WWTP effluent	This study
Calcined Pyroaurite	78.0	0 - 35	Phosphate synthetic solution	(Sun et al., 2013)
Calcined waste eggshells	31.7	0 - 112	Phosphate synthetic solution	(Panagiotou et al., 2018)
Zr-loaded Ca-montmorillonite	22.4	0 - 45	Phosphate synthetic solution	(Zou et al., 2020)
Thermally treated concrete	7.03	0 - 300	Phosphate synthetic solution	(Kang et al., 2017)
Iron oxide-coated GACs	10.8	0 - 90	Phosphate synthetic solution	(Kumar et al., 2017)
Zr-modified corn straw	29.3	0 - 30	Phosphate synthetic solution	(Hu et al., 2020)
Calcium Aluminate CaH_{10}	79.4	0-90	Phosphate synthetic solution	(Cheng et al., 2023)
Zr/MgFe-LDH	58.6	0-50	Phosphate synthetic solution	(Nuryadin et al., 2021)
Ca-Fe 2:1 LDH	47.7	0 - 20	Phosphate synthetic solution	(Ashekuzzaman and Jiang, 2014)
Mg-Al 2:1 LDH	76.1	0 - 70	Phosphate synthetic solution	(Zhang et al., 2019)
Mg-Al 3:1 LDH	98.3	0 - 40	Phosphate synthetic solution	(Liu et al., 2019)
Mg-Al 4:1 LDH	0.28	0 - 3	Phosphate synthetic solution	(Halajnia et al., 2013)
Zn-Fe 2:1 LDH	36.0	0 - 120	Phosphate synthetic solution	(Gupta et al., 2020)

Table S3. Parameters obtained from the fluid-dynamic characterization of the lab-scale and the pilot-scale columns packed with calcined pyroaurite.

Parameter	**Units**	**Lab scale**	**Pilot scale**
Bed height	m	0.20	0.60
EBCT	min	5	5
vs	m h^{-1}	2.4	7.2
As	--	3.2	2.4
HETP	mm	20	17
HETP/d_p	--	37	33

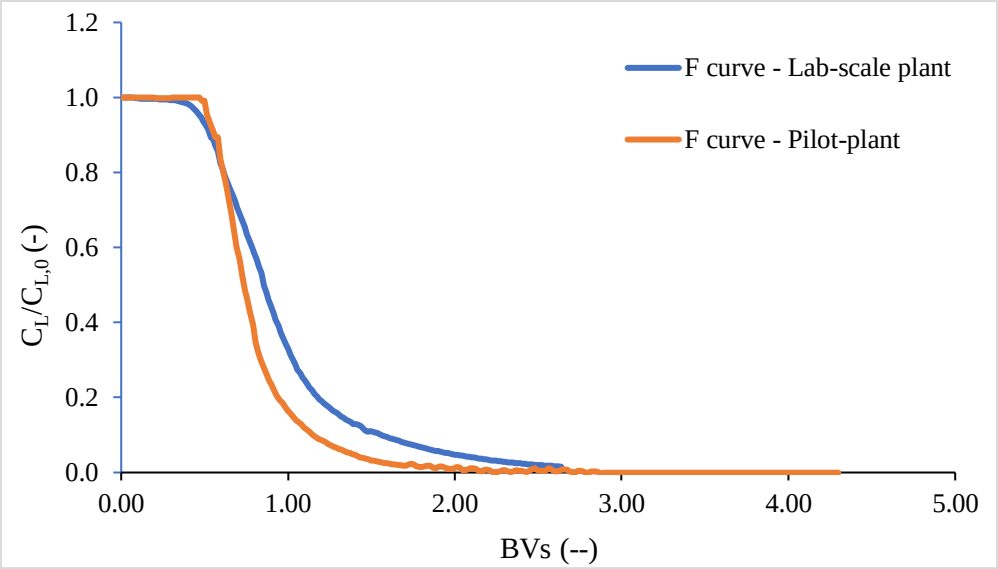

Figure S1. Comparison of the experimental curves obtained in the frontal analysis tests (step change in concentration) carried out to characterize the fluid dynamic behavior of the lab-scale 20-cm column (blue) and the 60-cm column placed in the pilot-plant (orange).

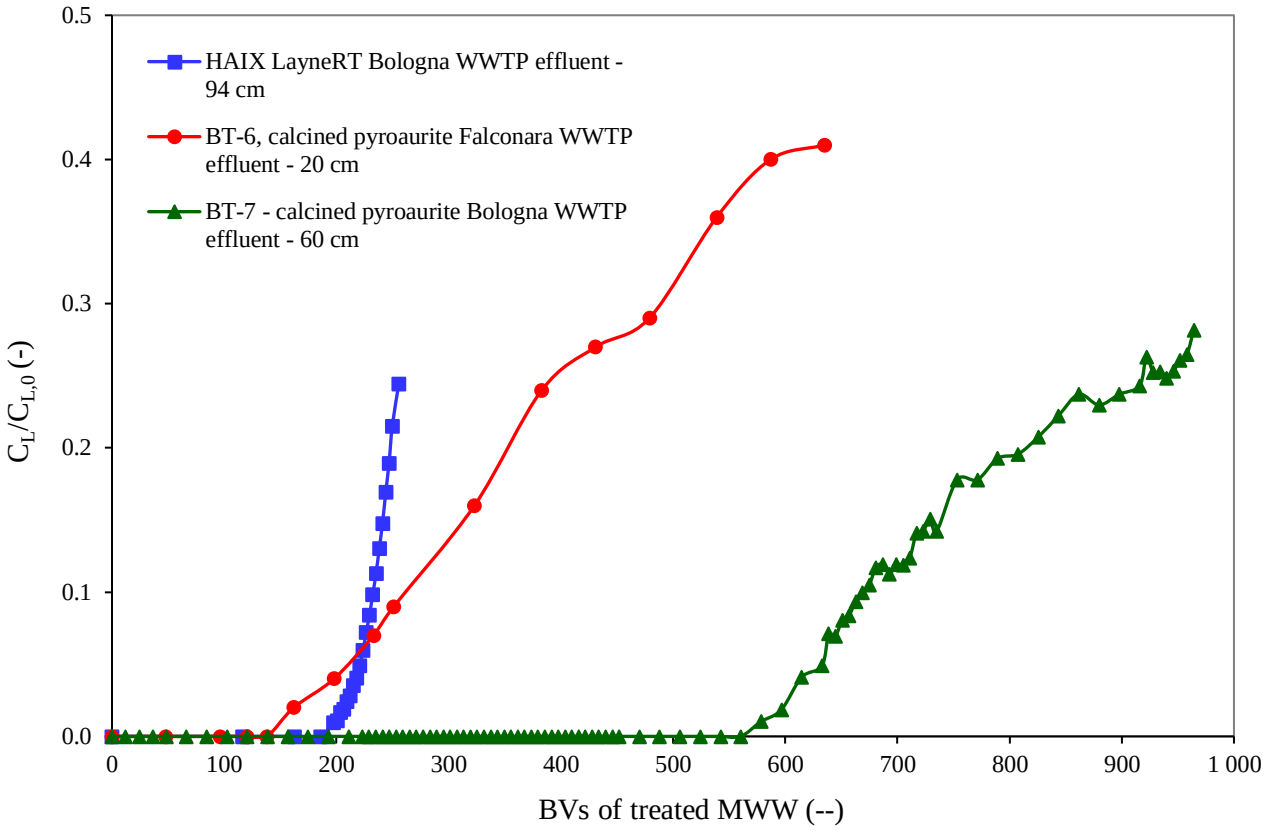

Figure S2. P adsorption breakthrough curves obtained with i) calcined pyroaurite in the 20-cm column fed with Falconara WWTP effluent (BT6 – red circles), ii) calcined pyroaurite in the 60-cm column fed with Bologna WWTP effluent (BT7 – green triangles), and iii) LayneRT in the 94-cm column fed with Bologna WWTP effluent (blue squares).

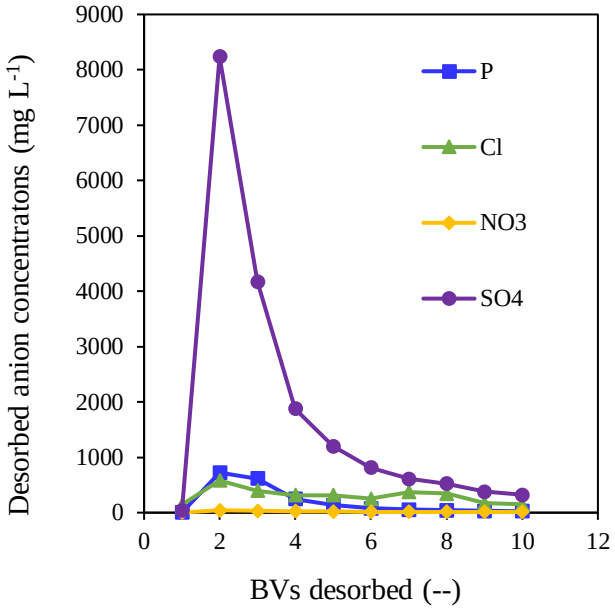

Figure S3. LayneRT breakthrough desorption curves in the pilot-scale 94-cm column fed with Bologna WWTP effluent spiked at 7 mg_P L^{-1}.

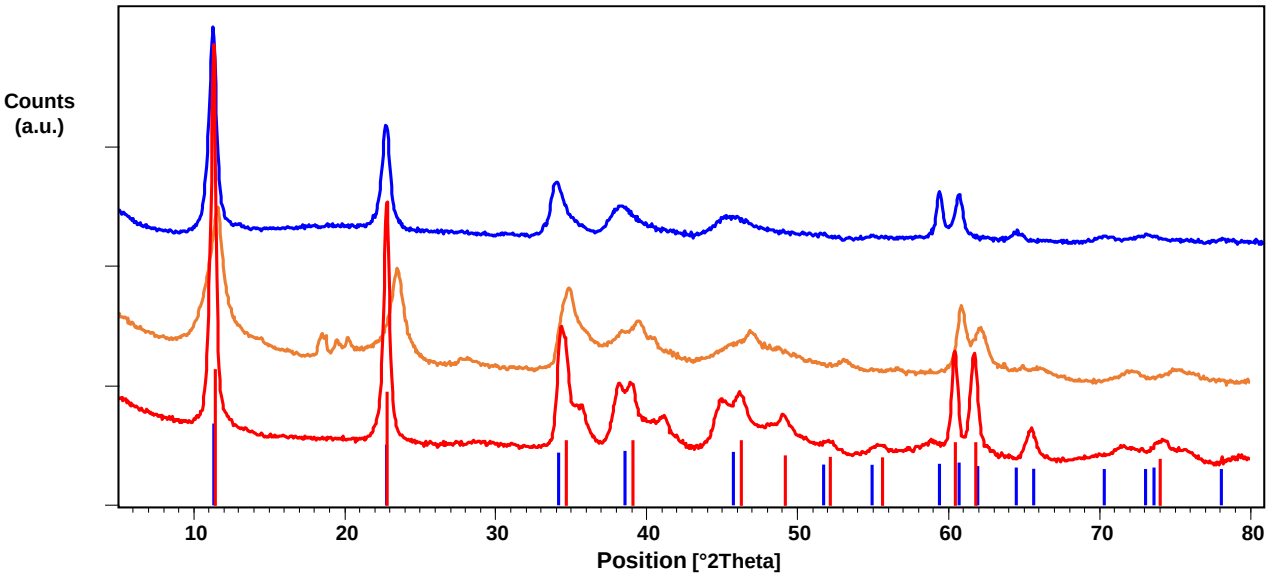

Figure S4. XRD diffractograms of hydrotalcite Pural 70 (red), hydrotalcite Pural 50 (orange) and synthesized virgin pyroaurite (blue). The reference patterns are shown as vertical line for hydrotalcites (red lines, PDF Ref. Code: 00-014-0191) and virgin pyroaurite (blue lines, PDF Ref. Code: 00-024-1110).

References cited in the Supplementary Material

Ashekuzzaman, S.M., Jiang, J.-Q., 2014. Study on the sorption–desorption–regeneration performance of Ca-, Mg- and CaMg-based layered double hydroxides for removing phosphate from water. Chemical Engineering Journal 246, 97–105. https://doi.org/10.1016/j.cej.2014.02.061

Cavani, F., Trifirò, F., Vaccari, A., 1991. Hydrotalcite-type anionic clays: Preparation, properties and applications. Catalysis Today 11, 173–301. https://doi.org/10.1016/0920-5861(91)80068-K

Cheng, P., Liu, Y., Yang, L., Ren, Q., Wang, X., Chi, Y., Yuan, H., Wang, S., Ren, Y.-X., 2023. Phosphate adsorption using calcium aluminate decahydrate to achieve low phosphate concentrations: Batch and fixed-bed column studies. Journal of Environmental Chemical Engineering 11, 109377. https://doi.org/10.1016/j.jece.2023.109377

Frascari, D., Bacca, A.E.M., Zama, F., Bertin, L., Fava, F., Pinelli, D., 2016. Olive mill wastewater valorisation through phenolic compounds adsorption in a continuous flow column. Chemical Engineering Journal 283, 293–303. https://doi.org/10.1016/j.cej.2015.07.048

Gupta, N.K., Saifuddin, M., Kim, S., Kim, K.S., 2020. Microscopic, spectroscopic, and experimental approach towards understanding the phosphate adsorption onto Zn–Fe layered double hydroxide. Journal of Molecular Liquids 297, 111935. https://doi.org/10.1016/j.molliq.2019.111935

Halajnia, A., Oustan, S., Najafi, N., Khataee, A.R., Lakzian, A., 2013. Adsorption–desorption characteristics of nitrate, phosphate and sulfate on Mg–Al layered double hydroxide. Applied Clay Science 80–81, 305–312. https://doi.org/10.1016/j.clay.2013.05.002

Hu, Y., Du, Y., Nie, G., Zhu, T., Ding, Z., Wang, H., Zhang, L., Xu, Y., 2020. Selective and efficient sequestration of phosphate from waters using reusable nano-Zr(IV) oxide impregnated agricultural residue anion exchanger. Science of The Total Environment 700, 134999. https://doi.org/10.1016/j.scitotenv.2019.134999

Kang, K., Lee, C.-G., Choi, J.-W., Hong, S.-G., Park, S.-J., 2017. Application of Thermally Treated Crushed Concrete Granules for the Removal of Phosphate: A Cheap Adsorbent with High Adsorption Capacity. Water Air Soil Pollut 228, 8. https://doi.org/10.1007/s11270-016-3196-1

Kumar, P.S., Prot, T., Korving, L., Keesman, K.J., Dugulan, I., Loosdrecht, M.C.M. van, Witkamp, G.-J., 2017. Effect of pore size distribution on iron oxide coated granular activated carbons for phosphate adsorption – Importance of mesopores. Chemical Engineering Journal 326, 231–239. https://doi.org/10.1016/j.cej.2017.05.147

Liu, C., Zhang, M., Pan, G., Lundehøj, L., Nielsen, U.G., Shi, Y., Hansen, H.C.B., 2019. Phosphate capture by ultrathin MgAl layered double hydroxide nanoparticles. Applied Clay Science 177, 82–90. https://doi.org/10.1016/j.clay.2019.04.019

Nuryadin, A., Imai, T., Kanno, A., Yamamoto, K., Sekine, M., Higuchi, T., 2021. Phosphate adsorption and desorption on two-stage synthesized amorphous-ZrO2/Mg–Fe layered double hydroxide composite. Materials Chemistry and Physics 266, 124559. https://doi.org/10.1016/j.matchemphys.2021.124559

Panagiotou, E., Kafa, N., Koutsokeras, L., Kouis, P., Nikolaou, P., Constantinides, G., Vyrides, I., 2018. Turning calcined waste egg shells and wastewater to Brushite: Phosphorus adsorption from aqua media and anaerobic sludge leach water. Journal of Cleaner Production 178, 419–428. https://doi.org/10.1016/j.jclepro.2018.01.014

Pinelli, D., Bovina, S., Rubertelli, G., Martinelli, A., Guida, S., Soares, A., Frascari, D., 2022. Regeneration and modelling of a phosphorous removal and recovery hybrid ion exchange resin after long term operation with municipal wastewater. Chemosphere 286, 131581. https://doi.org/10.1016/j.chemosphere.2021.131581

Sun, X., Imai, T., Sekine, M., Higuchi, T., Yamamoto, K., Akagi, K., 2013. Adsorption of Phosphate by Calcinated Mg-Fe Layered Double Hydroxide. J. of Wat. ^|^ Envir. Tech. 11, 111–120. https://doi.org/10.2965/jwet.2013.111

Zhang, Q., Ji, F., Zhao, T., Shen, Q., Fang, D., Kuang, L., Jiang, L., Ding, S., 2019. Systematic screening of layered double hydroxides for phosphate removal and mechanism insight. Applied Clay Science 174, 159–169. https://doi.org/10.1016/j.clay.2019.03.030

Zou, Y., Zhang, R., Wang, L., Xue, K., Chen, J., 2020. Strong adsorption of phosphate from aqueous solution by zirconium-loaded Ca-montmorillonite. Applied Clay Science 192, 105638. https://doi.org/10.1016/j.clay.2020.105638